Large Volume Nanoscale 3D Printing: Nano-3DP

Andrew I. M. Greer*[1], Emma Barbour[1], Marie F. Cutiongco[1], John M. Stormonth-Darling[1], Neil Convery[1], Rakan E. Alsaigh[2], Martin P.J. Lavery[2], Nikolaj Gadegaard*[1]

Affiliations:
[1]Division of Biomedical Engineering, School of Engineering, University of Glasgow, Glasgow, G128LT, UK.
[2]Structured Photonics Group, School of Engineering, University of Glasgow, Glasgow, G128LT, UK.

* E-mail: Andrew.Greer@Glasgow.ac.uk, Nikolaj.Gadegaard@Glasgow.ac.uk

Abstract: 3D printers suffer from the inverse relationship between throughput and minimum feature size; with smaller features inducing a cubic increase in print time. Here we introduce Nano-3DP, a hybrid process that combines digital light projection 3D printing with nanoscale-relief patterning. The tool enables large volume (cm^3) prints with nanoscale details at a truly rapid rate (~120 mm/hour). 40 nm features, half the size of the finest printed details to date, are produced across a scalable print volume. We address the intrinsic issues of throughput and pixel induced surface inhomogeneity. To demonstrate the unique potential realized by this printing method across different areas of science optical lenses, injection molding tools and bio-implants originally acquired by x-ray CT are produced with functional nanoscale surface details. Notably, *in vitro* bone cell analysis delivered a profound 4.5-fold increase in osteogenesis purely through the inclusion of nanoscale features on the printed surfaces.

Keywords: 3D printing additive manufacturing; nanofabrication; highest resolution; smallest feature; high throughput;

1. Introduction

3D printers have revolutionized design and manufacture processing in recent years. A diverse range of bespoke products have been produced to date from jewellery to vehicles.[*1-8*] Presently, a combination of printer affordability and reliability has enabled their deployment in the mass production of certain devices such as complex car parts, trainer mid-soles and cosmetic make-up brushes.[*9, 10*] Increasing the throughput and improving the resolution have been two of the primary areas of development. Although all forms of 3D printing are commonly referred to as rapid prototyping, digital light projection (DLP) vat polymerization is truly rapid and can print area independent volumes at around 100 mm/hour.[*11*] The throughput has been increased more than 10 fold via continuous liquid interface production (CLIP) to print in excess of 1000 mm/hour.[*11*] However both DLP and CLIP are limited in lateral resolution by the projected pixel size and a combination of the minimum controllable lift distance, resin viscosity and photo-sensitivity for vertical depths.[*12*] 4K high definition projection-based printers are currently being developed which push the minimal lateral resolution of DLP-based tools towards 20 μm^3 voxels [*13-15*]. Stereolithography (SLA), the scanning laser-based version of vat polymerization, although slower, is capable of printing finer details. The highest achievable resolution for SLA printing builds on the non-linear optical properties of 2-photon

polymerisation (2PP). One such setup uses a laser with a phase shifted and pulsed central column to provide a non-linear energy distribution within a highly localised volume to achieve the highest 3D printing fidelity.[*12, 16-21*] Many routes to further enhance the 2PP resolution have been explored. These include reducing the exposure wavelength,[*20*] synthesizing highly sensitive resins,[*22*] increasing scan speed,[*23*] reducing the volume of resin with the aid of scaffolds[*24, 25*] and post-print shrinkage.[*26*] Through a combination of these techniques, laboratory trials have demonstrated sub-80 nm line widths.[*22-26*] Evidently the wavelength dependence of 3D printing is now the limiting factor for feature definition. Even if 2PP or similar beam-based methods could define a smaller voxel, throughput would reduce cubically. Hence improving the resolution for DLP printers, whilst maintaining their high throughput, is a more attractive route for breaking the throughput / resolution inversion. Here we draw on experience and processes from microfabrication to combine large area and high throughput DLP 3D printing with nanoscale relief patterning, here after referred to as Nano-3DP.

The novelty of this work lies in realizing the printing method, Nano-3DP. The Nano-3DP tool brings together DLP-based 3D printing whilst simultaneously superimposing nanopatterns on the printed parts. This hybrid printing method benefits from large and fast volume printing yet provides surface detail not available by any 3D printing method today. It may be more accurately described as a surface processing extension of DLP printing. Critically, the extension capitalizes on the rapid, large volume print speed of DLP whilst processing surface details smaller than those achieved with 2PP systems. DLP is a truly rapid method of 3D printing where a vat of polymer resin has entire cross-sections cross-linked via optical exposure before the build plate lifts to expose the next layer. Here we have used electron beam lithography (EBL) coupled with reactive ion etching (RIE), capable of high precision depth control (+/-5 nm),[*27, 28*] to realize nanopatterns on the base of the resin basin, **Figure 1 (a-b)**. It was determined that polydimethylsiloxane (PDMS) replicas of etched Si masters is the most effective means of nanoscale pattern transfer between the basin and the printed surface. Every layer printed in the basin will be subject to relief molding of the basin nanotopography. Nano-3DP compliments the existing technologies on these terms as shown in **Figure 1 (b)**.

2. Results and Discussion

2.1 Nano-3DP capacity: The smallest 2PP features to date were produced by Xing *et al*. by incorporating a highly sensitive and efficient photo-initiator into their resin to best match their radiation source, coupled with a rapid scan speed of 50 µm/s they were able to take advantage of the non-linear energy distribution within the laser spot to achieve optimum printing of ~1/10 λ, 80 nm.[*23*] The features produced using the Nano-3DP tool are half the size of this, whilst matching the rapid layer printing speed of DLP. **Figure 1 (c-d)** show circular features of ~40 nm diameter on the Nano-3DP basin and the relief in a polymer print respectively. 40 nm lateral dimensions were the smallest features tested here, the X/Y resolution may be even finer dependent on the fidelity of the e-beam and RIE processing of the master. A limitation of both two-dimensional UV-NIL and this here three-dimensional hybrid system is that the nanofeatures are pre-defined. This does not however restrict every layer of the print to the same design; sequential layers may have the nanostructures changed between exposures as shown in **Figure 1 (f-g)**. Here the basin was repositioned between layers so that gratings could be printed on different layers at different angles. The minimum layer thickness produced using the Nano-3DP

set-up reported here is ~4.5 µm (**Figure S1**), which is on par with state of the art DLP systems,[*13*] and takes just 600 ms to expose. The area of the exposure is independent of the curing time but rather defined by the area of the projection source. Thus, large area nanostructured prints may be achieved in a matter of seconds with a throughput of ~120 mm/hour. 1000-layer prints were produced with the tool without degradation of the PDMS nanopattern. We have previously shown that fluorinated polymer surpasses PDMS nanoimprint performance, 1000-fold, thus would further improve the printing capacity of Nano-3DP should a custom vat be fabricated from such a polymer.

2.2 Nanoscale fidelity: Although the nanoscale surface features are here achieved via relief patterning of the area exposed by DLP pixels, Sun *et al*. documented that the energy distribution of a digital pixel may be approximated by a first order Gaussian point spread function.[*29*] Thus when pixel arrays, like those used in DLP printers, are deployed to cross-link resin the printed surface is not planar but textured by the Gaussian distributed beams, as shown in **Figure 2 (a) & (b)**. In these optical profilometry reconstructions, the 150 µm square pixels of the projector used in this work are shown to increase the printed surface in height by 3.5 µm towards the centre point. Such microscale artifacts may compromise the functionality of some printed nanotopographies, such as optical gratings (**Figure 2 (c)**). We demonstrate how these Gaussian swells may be alleviated in **Figure 2 (d) & (e)** through defocusing of the projector during printing and that indeed the issue of laser light diffusing when passing through the printed optics is remedied (**Figure 2 (f)**). **Figure 2 (g)** graphs the effect of focal position on surface roughness. Despite an intrinsic size increase with defocused projections, the projected shape is not significantly affected (**Figure S4**). Thus, it is possible to trade off projection size for a smoother surface finish by accounting for the size change during the design stage. 15 mm of defocus can reduce the average surface roughness by over 50% to sub-1 µm yet the feature shape remains in the 99th percentile. Presently freeform optical elements are typically produced by diamond turning poly(methyl methacrylate) (PMMA),[*30*] which limits low cost reproduction. 3D printing allows the rapid and economical printing of optical elements from a digital design file, with geometries readily tuned for different experimental set-ups in labs worldwide. We used the Nano-3DP tool to print a mode transformer. **Figure 2 (i)** shows the element with a 0.5 mm deep groove. Additionally, we used the printer to incorporate a 325 nm deep binary grating to integrate an optical fan-out for high efficiency optical transformation.[*31*] The Nano-3DP tool does not only improve manufacturability and distribution of this lens, but also the experimental set-up is simplified by the intrinsic hierarchical fusion of the nanograting with the microgroove. This tool has the potential to manufacture novel optics that cannot be produced otherwise, and the resin may be varied during printing to localize resin parameters between sections of the print. This may be observed in **Figure 2 (i)**, where switching the resin mid-print was a requirement to vary the transparency between the lens and the housing for safe control of optical transmission. To switch the resin printing was simply paused and the vat replenished with a different resin.

2.3 Manufacture scalability: Today, 3D printers are synonymous with rapid prototyping unique devices, the affordability and speed of the current printers has enabled their introduction to the field of mass production. In 2018 DLP printers were used by Carbon to produce 200,000 mid-soles for Adidas shoes which featured a complex design not achievable via traditional manufacturing techniques.[*10*] Although the Nano-3DP set-up presented here is DLP-based, we further demonstrate that traditional manufacturing systems such as injection molding may be

coupled with this printer to rapidly generate tools. This improves efficacy for tool design, in particular with reference to producing and refining tools for nanoscale molding where definition of nanopatterns on non-planar surfaces remains highly stringent and time intensive for rudimental structures.[*32, 33*] Originally tools for injection molding are machined from metal which is much slower than direct 3D printing and is further limited by the microscale resolution of CNC tooling. In order to realize the optimum conditions for injection molding, many iterations of tool design and tweaking of the process parameters are required. Here, injection molding tools were printed on the Nano-3DP using various polymer resins documented in the supplementary pages. The printed tools withstood a melt temperature of 260 °C and hold pressure of 800 bar using an Engel Victory 28 commercial injection molding machine. The molded parts replicated nanotextured 3D prints of 240 nm depth (**Figure S5)**. The only other 3D printing method capable of printing channels of this scale is 2PP, but the serial exposure of voxels does not bode efficacious for even relatively small injection molding tools. **Figure 3** highlights the feedback-loop process of nanoscale tooling for injection molding expedited by the inclusion of the Nano3DP**.**

2.4 Novel applications: Nano-3DP enables a variety of novel applications with higher resolution surface details than currently available. Besides engineering applications, 3D printing is seeing a rapid growth in regenerative medicine.[*34*] 3D printing is the clinicians' tool of the future which is already being paired with computed tomography (CT) scanners to enable a physician to custom design an implant to accurately fit the existing tissue geometry of the patient,[*35*] **Figure 4**. The Nano-3DP tool further facilitates the nanopatterning of the printed implant. This is beneficial as it has been widely reported that surface texture can accurately control stem cell fate. [*36-39*] A visual example of cells responding to the printed nano-textured surfaces may be found in the supplementary pages (**Figure S2**). The Nano-3DP tool is evidently able to print custom sized devices with bioactive nanotopographies to better aid patient recovery. Bioactive nanotopographies, which up-regulate bone tissue regeneration, [*36-41*] were patterned onto CT scan generated prints using the Nano-3DP tool, **Figure 4**. Here MC3T3 osteoblast precursor cells have been cultured for 14 days upon Transparent Custom Resin 3D prints; one with, and one without the nanotopography. A highly significant ($P < 0.001$) 4.5 fold up-regulation in osteopontin, a protein known to be associated with the early stages of bone formation,[*42*] was observed on the nanopatterned print **Figure 4 (f)**. Such a profound biological response without additional materials, proteins or chemical catalysts truly highlights the significant impact this nanopatterning / 3D printing fusion enables. The contrast in biological response may be observed clearly in **Figure 4 (e-g).** These composite images, produced using three different light sources to excite three different fluorescent stains, show the level of OPN bone protein (green) produced on each surface as well as the cell cytoskeleton (red) and nucleus (blue).

3. Conclusions

In conclusion we have demonstrated rapid 3D printing of large volume, high throughput structures with higher detail than previously possible. The optical wavelength dependence of 3D printers is here overcome by fusing nanoimprint with digital light projection to realize Nano-3DP. The nanopatterns are produced using electron beam lithography and reactive ion etching so features far smaller than those possible with any other light-based printer are now readily obtainable. Here ~4.5 µm thick layers are printed in under a second containing surface features down to 40 nm diameter. This is half the size of the smallest lateral spatial resolution possible

with fully optimized two-photon polymerization. This Nano-3DP tool enables throughput several orders of magnitude higher than multi-beam and thermal filament printers. Both commercial and mixed resins were demonstrated to be effective in replicating nanopatterns from the predefined topographies on the resin basin. In particular, the Transparent Custom Resin is of significance due to its biocompatible and transparent properties. These have allowed applications in both optics and regenerative medicine to be demonstrated. With the later we have demonstrated a highly significant, 4.5-fold, increase in osteogenic bioactivity entirely as a result of printing nanopits on the substrates via the Nano-3D Printer. Furthermore, nanotextured prints may also be readily mass produced via replication with injection molding machines. Both resins tested in this work may be utilized for rapidly printing injection molding tools; where otherwise tool development, especially in the nanoscale domain, are costly and time consuming. Here gratings down to 240 nm were printed in combination with microfluidic channels to demonstrate how a simple fluidic filter may be achieved with channel sizes below those possible via traditional projection-based 3D printers.

4. Materials and Methods

4.1 Preparing the nano patterns: There are three predominant routes each utilizing three different media for generating nanopatterned basins: glass etching, polydimethylsiloxane (PDMS) bonding and molding plastics. In this work injection molded polystyrene was found to foul rapidly within 20-layer prints. Glass etching is not scalable and was not evaluated. Fluorinated polymers presented bonding failures due to their non-stick nature. Cast PDMS bonded to polystyrene petri dishes was found to be the most effective for 1000-layer prints and is readily reproducible thus disposable thereafter. PDMS nanopatterns are produced by casting Sylgaard 184 in a 10:1 weight ratio onto a predefined nano-mold. In this work fluoro-silane terminated etched Si moulds defined by conventional electron beam lithography processes are used. The cast PDMS is degassed and cured at 70 °C for 2 hours before being demolded. The PS petri dish is exposed with oxygen plasma to activate the surface for bonding. More PDMS of the same mix is then used as an adhesive to mount the nanopatterned layer in the dish. The dish is left to cure for a further 2 hours.

4.2 Tool construction: The printer was constructed using off-the-shelf components to readily facilitate open access to the technology. A Windows PC runs Creation Workshop (or alternative DLP freeware) and communicates with an Arduino controlled stepper motor mounted on an aluminum X-bar frame. The motor drives a spindle gear that lowers and raises a 25 mm diameter aluminum build plate. Mid-frame sits a platform for pinning a 40 mm diameter petri-dish. Below the petri-dish is a 45-degree mirror. A high definition desktop projector with its UV filter removed is connected to the PC graphics card. Projected images are focused using the projector focus ring onto the base of the petri-dish via the 45-degree mirror.

4.3 Resins: In this work several commercial resins were evaluated but only one exhibited functional characteristic for replicating nanotopographies, Industrial Blend 1B (Black) from Fun To Do (referred to in the text as Black Commercial Resin). This resin contains sub-micron particles which provide mechanical integrity to nanoscale structures and contribute towards the black color which itself reduces light bleed and increases fidelity. 150 nm diameter features were faithfully reproduced from PDMS resin basins. This proprietary resin is however toxic and thus

not suitable for biological applications. A specifically designed biocompatible transparent resin based on PEG-DA (MW 250 Da) was prepared following a custom recipe developed and documented in the work by Urrios *et al.* as follows: PEG-DA-258 (Sigma Aldrich) mixed with 0.6% (w/w) Irgacure 819 (BASF Corporation) as a photoinitiator and 0.6% (w/w) 2-isopropylthioxanthone (ITX) as a photosensitizer, (*13*) (referred to in the text as Transparent Custom Resin). This resin was found to be highly effective for rapid (see print conditions below) printing of nanoscale surface features down to 40 nm diameter from PDMS resin basins.

4.4 Print conditions and post-processing: Lift 1.5 mm between each layer print at a lift rate of 200 mm/s. For Transparent Custom Resin , 6.5 µm slices expose for 1.0 second with three base layers at 1.1 second. For Industrial Blend 1B 100 µm slices exposed for 2.15 seconds with three base layers at 2.3 second. For biocompatibility the Transparent Custom Resin is required to be rinsed in water for 12 hours while simultaneously illuminating it with UV light. Followed by 2 minutes of 150 Watt oxygen plasma to provide a cell adhesive surface.

4.5 Cell culture experiments: MC3T3 osteoblast precursor cells were cultured in MEMα media with nucleosides and L-glutamine without ascorbic acid (Thermo Fisher Scientific) and supplemented with 1% penicillin-streptomycin (Sigma Aldrich) and 10% FBS (Thermo Fisher Scientific). Prior to cell seeding, the substrates were incubated in culture dishes with complete media for one hour. Cells were harvested from culture flasks using trypsin and spun at 300 x g for 5 minutes. MC3T3 cells were resuspended in complete media and seeded at 10,000 cells/cm^2 onto substrates. Cells were continuously monitored for 14 days, with media changes every 48 hours.

4.6 Immunofluorescence staining: Once cultured, the cells were fixed with 4% paraformaldehyde solution in PBS for 15 minutes at 4°C. The fixed cells were permeabilized with Triton-X in PBS, followed by blocking in 10% donkey serum and 2% bovine serum albumin in PBS for one hour at room temperature. The cells were stained with osteopontin (Abcam, ab8448, 1:200) overnight at 4°C. After overnight incubation Alexa Fluor conjugated secondary antibodies (Thermo Fisher Scientific) against the host species of primary antibody were used at 1:500 dilution. Simultaneously ActinGreen ™ 488 ReadyProbes ™ Reagent and NucBlue ™ Fixed Cell ReadyProbes™ Reagent (Thermo Fisher Scientific) were used to stain the actin cytoskeleton and nuclei respectively. Samples were mounted on 0.17µm glass coverslips with Prolong™ Gold Antifade Mountant (Thermo Fisher Scientific) and dried overnight at 4°C before imaging.

4.7 Fluorescence microscopy: Images were obtained using EVOS FL Auto 2 Cell Imaging System (Thermo Fisher Scientific) at 10x (EVOS AMEP-4623, 0.3NA) magnification. Cell Profiler was deployed to quantify the levels of OPN produced per surface. Bins of up to 10 images were used for statistical significance. Using intensity and area-based threshold masks, the number of nuclei and the area of OPN fluorescing pixels were evaluated. Dividing the OPN pixels by the total number of nuclei per image produced the mean value of OPN/cell. On average from bins of up to ten images the fold difference was 4.54 in favor of the nanopatterned surface with highly significant standard error.

4.8 Cell SEM preparation: Cells were fixed on the substrates using 1.5% glutaraldehyde in 0.1 M sodium cacodylate for 1 hour. The substrates were rinsed three times in 0.1 M sodium cacodylate for 5 minutes. The fixed cells were incubated in 1% osmium tetroxide for one hour and washed is ddH_2O three times for 10 minutes. Once washed the samples were incubated in 0.5% uranyl acetate for one hour and changed into ddH_2O. The samples were then dehydrated in the following series for 10 minutes at each step: 30% ethanol, 50% ethanol, 70% ethanol, 90% ethanol, absolute ethanol and dried absolute ethanol. Once dehydrated in ethanol the samples were subjected to critical point drying. Samples were subsequently sputtered coated with a mix of 80:20 - Au:Pd to act as a charge dissipation layer for SEM. (All chemicals listed in this section were purchased through Sigma Aldrich).

4.9 Injection molding: Polystyrene was molded in an Engel Victory 28 fully hydraulic injection moulding machine with the following settings: melt temperature - 260 ^oC, tool temperature – 20 ^oC, injection speed - 1 cm^3/s, shot volume - 4 cm^3, hold pressure – 800 bar, hold pressure time - 5 s, colling time - 15 s.

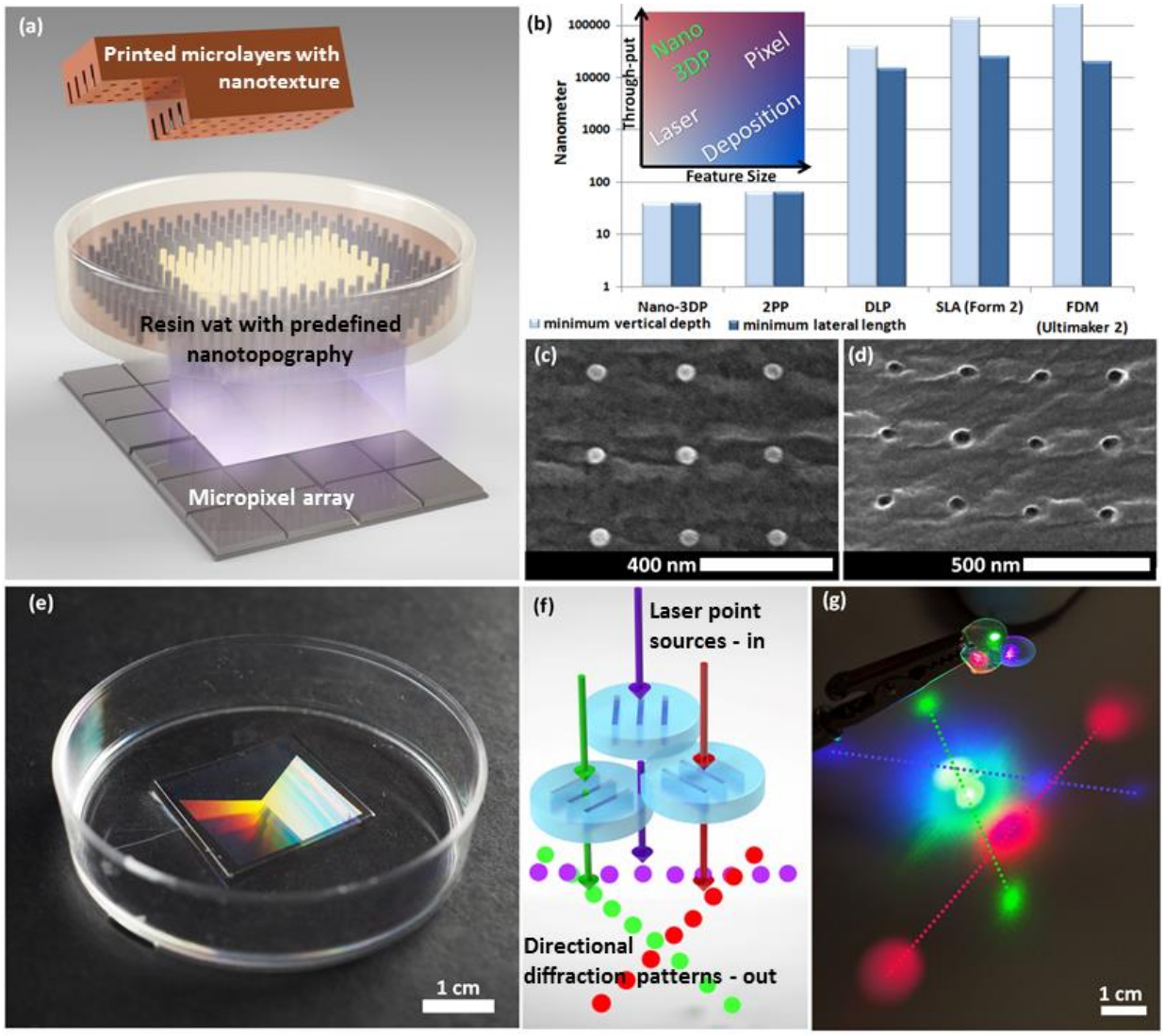

Figure 1. (a) 3D Rendered model of the Nano-3DP set-up with an e-beam defined nanopattern etched into the base of the DLP resin basin enabling sub-wavelength nanofeatures to be imprinted on each layer of the print. (b) Graph of feature sizes for comparable three-dimensional printer technologies (inset – quadrants achieved by existing technology, left to right: feature size, bottom to top: throughput). (c) Electron micrograph of ~40 nm diameter PDMS pillars on a resin basin. (d) The resultant ~40 nm diameter pits in a Transparent Custom Resin print from the basin pillars shown in part '(c)'. (e) A photograph of an exemplary nanopatterned transparent resin basin. (f) Each layer may be printed with a different nanotopography by changing the basin pattern between exposures, laser light may be deployed to confirm the presence of nanopatterns, especially on transparent prints. (g) Photograph of a three-stage-print with nanogratings running in different directions on each stage. Three colored laser beams shining through each stage are here shown to generate diffraction patterns in mutually exclusive directions.

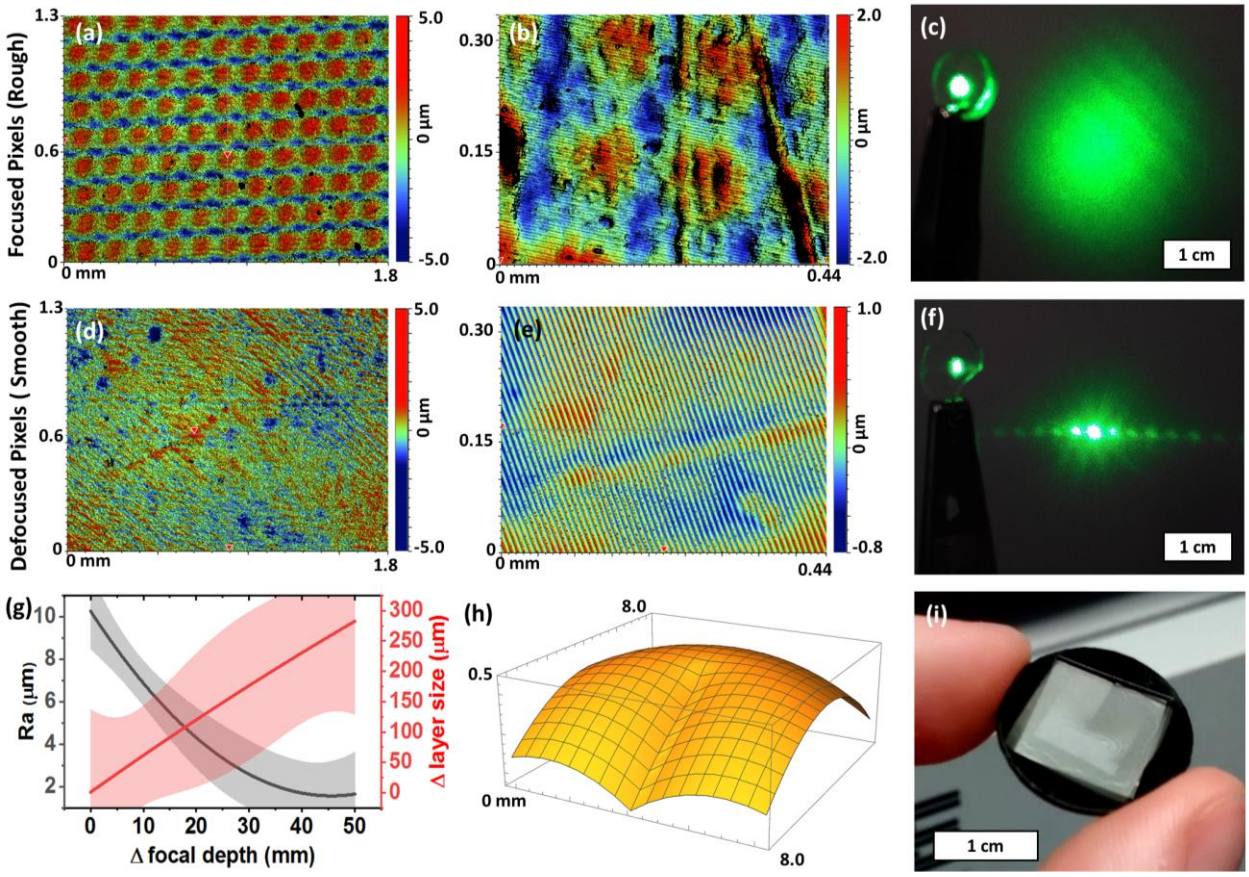

Figure 2. (a-b) Optical profilometer reconstruction of a printed surface displaying the 3.5 µm deep Gaussian shaped pixel artifacts disrupting the 300 nm deep, 8 µm wide binary grating. (c) Photograph of a lens printed with focused pixels shown to diffuse laser light. (d-e) The optical profile reconstruction of the nanograting surface printed with 50 mm defocused pixels showing a smoother microscale surface. (f) Photograph of a lens printed with defocused pixels functioning effectively to diffract the light. (g) Graph of average surface roughness (black) and average change in layer size (red) against focal position where 0 mm represents light in focus on the base of the resin basin and bands represent 95% confidence fitting. (h) CAD model of micro-groove lens. (i) The printed lens in Transparent Custom Resin bonded to a carrier ring in Black Commercial Resin. The Nano-3DP basin featured 300 nm deep gratings running orthogonal to the micro-cress of the lens and are visible as a lighter 1x1 cm^2 area in the center of the lens.

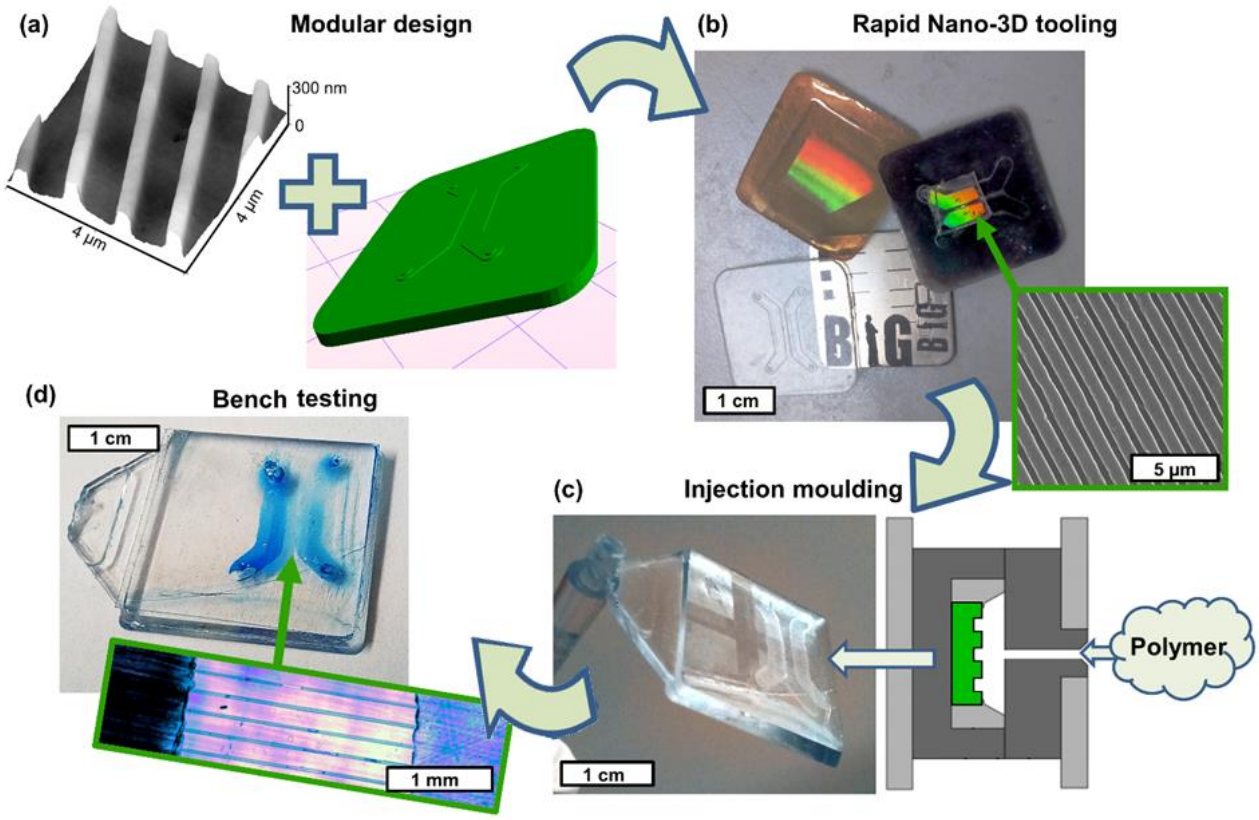

Figure 3. (a) the modular approach of fusing pre-defined nano/micropatterns upon resin vats with macroscale stereolithography designs realizes injection molding tools with features 500-fold smaller than tools printed with conventional DLP 3D printers. (b) Nano-3DP printed injection molding tools on various resins (see supplementary) exhibiting a range of material properties; the transparent tool shows two parallel 1 mm deep microfluidic cavities, the translucent tool contains a micro grating and the black tool fuses these two designs so that the micro-grating channels run orthogonally across the millimeter cavities, thus creating the mold for a fluidic filter. (c) cross-section schematic of how the 3D tool is housed during injection molding and a photograph of a polystyrene part produced via injection molding against a printed Nano-3DP printed tool. (d) the injection molded part has been sealed over with a polystyrene sheet to complete the microfluidic filter. Isopropyl alcohol mixed with blue food coloring was injected into the filter, an optical micrograph of the fluidic channels is displayed.

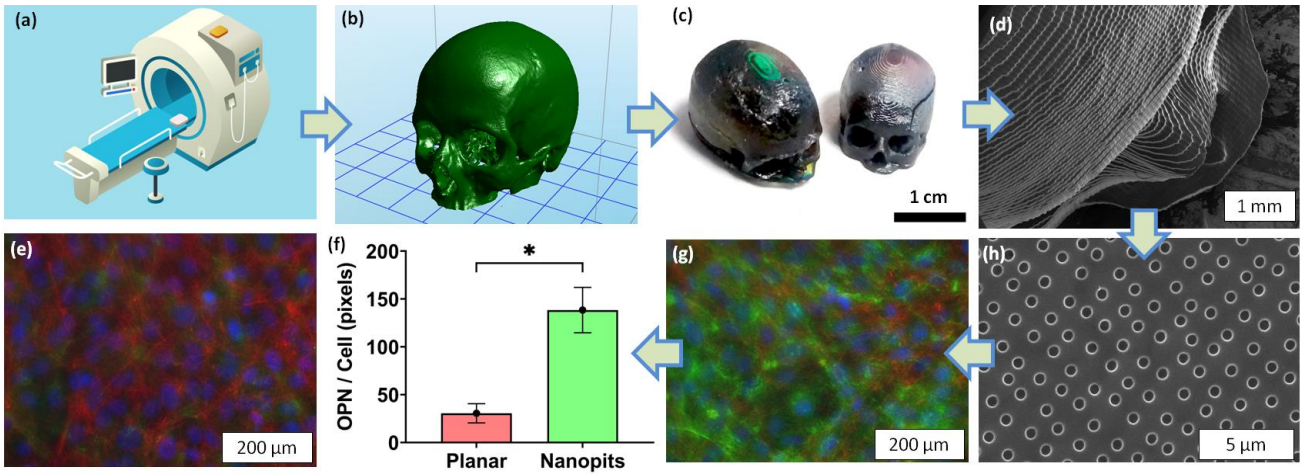

Figure 4. (a) Using a CT, MRI or X-Ray scanner it is possible to generate stereo lithography models. (b) Stereolithography model of a human skull generated from a CT scan. (c) Photograph of printed ~1 cm^3 skulls in Black Commercial Resin where colored interference patterns can be seen at the top and bottom of the print due to the imprinted nanopatterns. (d) SEM top-down image of one of the skulls from part (c) where 40 µm thick print layers are visible. (e) Optical micrograph of mouse pre-osteoblast cells fluorescently stained for nuclei (blue), actin (red) and osteopontin bone protein (green) after being cultured for 14 days on a planar printed PEG-DA control surface. (f) Bar chart quantifying the highly significant (p-value <0.001) level of osteopontin bone protein produced by prints with nanopits relative to planar surfaces both produced on the Nano-3DP tool. (g) The same image as part (e) except the printed surface is not planar, it features the osteoinductive nanopattern shown in (h). (h) Close-up SEM of the osteoinductive nano-pits on the surface of the printed skulls shown in (c) and (d).

References:

[1]. K. Sun *et al.*, *Advanced materials* **25**, 4539 (2013).
[2]. C. Zhu *et al.*, *Nano Letters* **16**, 3448 (2016).
[3]. D. Zhang *et al.*, *Synthetic Metals* **217**, 79 (2016).
[4]. W. Bao *et al.*, *Advanced materials* **28**, 4684 (2016).
[5]. Y. Yao *et al.*, *ACS nano* **10**, 5272 (2016).
[6]. J. Kietzmann, L. Pitt, P. Berthon, *Business Horizons* **58**, 209 (2015).
[7]. C. L. Ventola, *Pharmacy and Therapeutics* **39**, 704 (2014).
[8]. J. Bargmann, *Popular Mechanics*, (2013).
[9]. P. Ray, Y. Rao, *Advance and Innovative Research*, 80 (2019).
[10]. J. M. Jordan, *Journal of Organization Design* **8**, 5 (2019).
[11]. J. R. Tumbleston *et al.*, *Science* **347**, 1349 (2015).
[12]. J. W. Stansbury, M. J. Idacavage, *Dental Materials* **32**, 54 (2016).
[13]. A. Urrios *et al.*, *Lab on a Chip* **16**, 2287 (2016).
[14]. C. S. Favero *et al.*, *American Journal of Orthodontics and Dentofacial Orthopedics* **152**, 557 (2017).
[15]. N. Bhattacharjee, C. Parra-Cabrera, Y. T. Kim, A. P. Kuo, A. Folch, *Advanced materials* **30**, 1800001 (2018).
[16]. S. Kawata, H.-B. Sun, T. Tanaka, K. Takada, *Nature* **412**, 697 (2001).
[17]. F. P. Melchels, J. Feijen, D. W. Grijpma, *Biomaterials* **31**, 6121 (2010).
[18]. M. T. Raimondi *et al.*, *Journal of applied biomaterials & functional materials* **10**, 56 (2012).
[19]. S. Waheed *et al.*, *Lab on a Chip* **16**, 1993 (2016).
[20]. N. Bhattacharjee, A. Urrios, S. Kang, A. Folch, *Lab on a Chip* **16**, 1720 (2016).
[21]. K. Obata, A. El-Tamer, L. Koch, U. Hinze, B. N. Chichkov, *Light: Science & Applications* **2**, e116 (2013).
[22]. J. Xing *et al.*, *Journal of Materials Chemistry B* **3**, 8486 (2015).
[23]. J.-F. Xing *et al.*, *Applied physics letters* **90**, 131106 (2007).
[24]. W. Haske *et al.*, *Optics express* **15**, 3426 (2007).
[25]. D. Tan *et al.*, *Applied physics letters* **90**, 071106 (2007).
[26]. D. Oran *et al.*, *Science* **362**, 1281 (2018).
[27]. I.-B. Baek *et al.*, *Journal of Vacuum Science & Technology B: Microelectronics and Nanometer Structures Processing, Measurement, and Phenomena* **23**, 3120 (2005).
[28]. W. Chen, H. Ahmed, *Journal of Vacuum Science & Technology B: Microelectronics and Nanometer Structures Processing, Measurement, and Phenomena* **11**, 2519 (1993).
[29]. C. Sun, N. Fang, D. Wu, X. Zhang, *Sensors and Actuators A: Physical* **121**, 113 (2005).
[30]. M. P. Lavery *et al.*, *Optics express* **20**, 2110 (2012).
[31]. G. C. Berkhout, M. P. Lavery, J. Courtial, M. W. Beijersbergen, M. J. Padgett, *Physical review letters* **105**, 153601 (2010).
[32]. Y. Zhang, D. B. Pedersen, A. S. Gøtje, M. Mischkot, G. Tosello, *Journal of Manufacturing Processes* **27**, 138 (2017).
[33]. J. M. Stormonth-Darling, A. Saeed, P. M. Reynolds, N. Gadegaard, *Macromolecular materials and engineering* **301**, 964 (2016).
[34]. S. Patra, V. Young, *Cell biochemistry and biophysics* **74**, 93 (2016).
[35]. P. Canzi *et al.*, *Acta Otorhinolaryngologica Italica* **38**, 251 (2018).

[36]. M. J. Dalby, N. Gadegaard, R. O. Oreffo, *Nature materials* **13**, 558 (2014).
[37]. T. Sjöström, L. E. McNamara, R. Meek, M. J. Dalby, B. Su, *Advanced healthcare materials*, (2013).
[38]. R. K. Jaiswal *et al.*, *Journal of Biological Chemistry* **275**, 9645 (March 31, 2000, 2000).
[39]. M. J. Biggs *et al.*, *Biomaterials* **30**, 5094 (2009).
[40]. L. E. McNamara *et al.*, *Biomaterials* **32**, 7403 (2011).
[41]. N. Gadegaard, M. J. Dalby, M. O. Riehle, C. D. Wilkinson, *Journal of Vacuum Science & Technology B: Microelectronics and Nanometer Structures* **26**, 2554 (2008).
[42]. D. T. Denhardt, X. Guo, *The FASEB journal* **7**, 1475 (1993).
[43]. L. L. Chiu, K. Janic, M. Radisic, *The International journal of artificial organs* **35**, 237 (2012).

Acknowledgments: We acknowledge ERC funding through FAKIR 648892 Consolidator Award. MFAC is financially supported by the University of Glasgow MG Dunlop Bequest, College of Science and Engineering Scholarship, and FAKIR consolidator award. NG acknowledges support by the Research Council of Norway through its Centres of Excellence funding scheme, project number 262613. This work was supported by the Engineering and Physical Sciences Research Council [EPSRC) grant EP/N5096681/1. We acknowledge the James Watt Nanofabrication Center for fabrication work.

Supplementary Materials:

Desktop 3D printers boast a minimum layer thickness of 5 µm**, Figure S1** shows a profile scan highlighting the capacity of the Nano-3DP tool to print layers approaching 4.5 µm in depth. This indicates that despite off-the-shelf components, the simplistic stepper spindle configuration driven by an Arduino controller can achieve layer depths on par with commercial tools. Trivially thin layers result in lower throughput, but higher detailing.

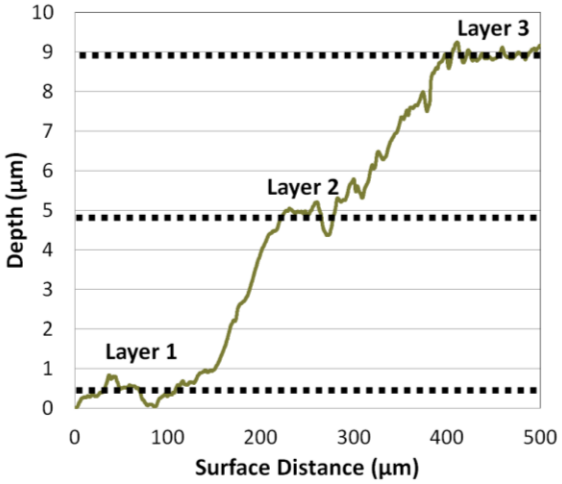

Figure S1. Surface profile of ~4.5 µm layer steps printed with the Nano-3DP tool.

Figure S2 is evidence that Nano-3DP is capable of printing biocompatible material with nanotopographical cues. The images sequentially show increased magnification of 10 µm deep printed layers featuring 150 nm deep grooves on the surface. Such grooves are useful in regenerative medicine for aligning cells. Such scaffolds are important for enhancing the speed that cardiomyocyte cells form synchronized beating.(*43*) Additionally, **Figure S2** shows that the nanofeatures may be varied or renewed between printed layers without producing boundary artifacts. This is useful for complex interfaces, such as between fixed and articulating surface or simply where fouling of the nanopattern is a concern due to continual large volume printing.

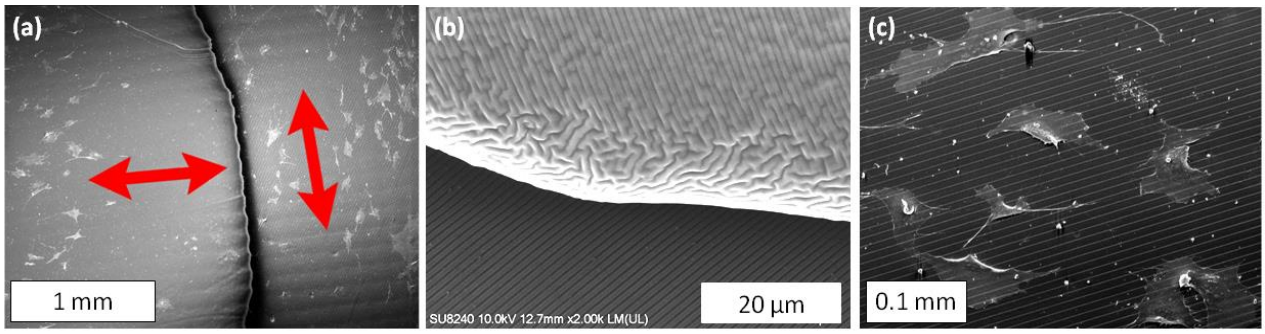

Figure S2. (a) Electron micrograph of a PEG-DA printed 10 µm layer step where the imprinted nanograting is orthogonal on each layer, the direction of the gratings is highlighted by the arrows. The cells cultured for 1 day on the sample are shown to align to the plane of the grating. (b) Close-up SEM of a layer boundary where the top layer has orthogonal nanogratings to the lower layer. (c) Mouse pre-osteoblast cells aligning to a 4 µm wide, 150nm deep imprinted grating.

To exemplify the fact that the custom-built Nano-3DP tool is functional with commercial resins, Industrial Blend 1B from Fun To Do was tested. The black version is a suspension of carbon nanoparticles so has higher fidelity than alternative colors in this range. **Figure S3** shows the smallest nanopillars of 150 nm diameter protruding from the surface of a print produced on the Nano-3DP tool using said black acrylate-based resin.

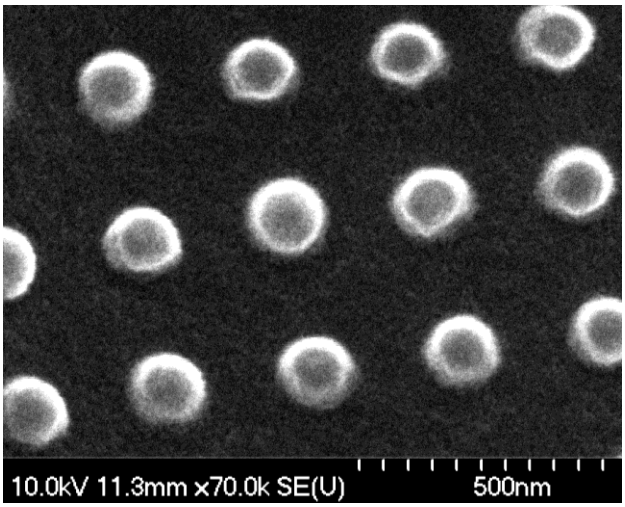

Figure S3. 150 nm diameter pillars protruding from the surface of a Nano-3DP print using Industrial Blend 1B resin from Fun To Do.

Defocusing the projected pixels on the bottom of the resin basin is able to improve the surface finish. The printed layers did increase in lateral size with defocus, however circular layers were found to retain strong circularity. **Figure S4** plots the change in circularity against defocus. Figure S3 indicates that 15 mm of defocus is possible without any impact on the layer shape. Thus smoother surface finishes may be generated without adverse effect on the macro layer shape.

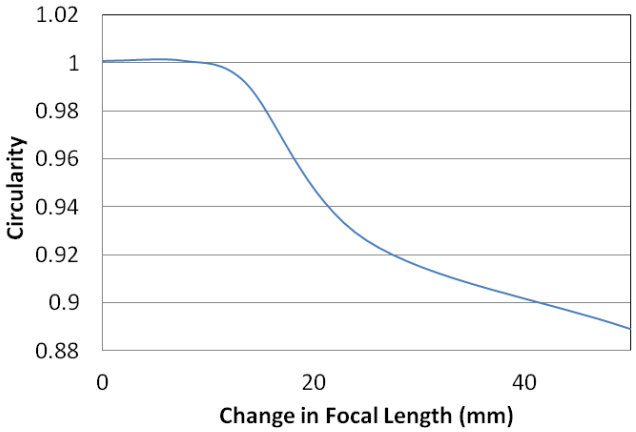

Figure S4. Printed layer circularity plotted against focal displacement where 0 mm corresponds to the printer being in focus.

Injection molding fidelity of nanostructures was evaluated via SEM and AFM inspection of the 3D printed mold against the polystyrene replica. Figure S5 shows the faithful replication.

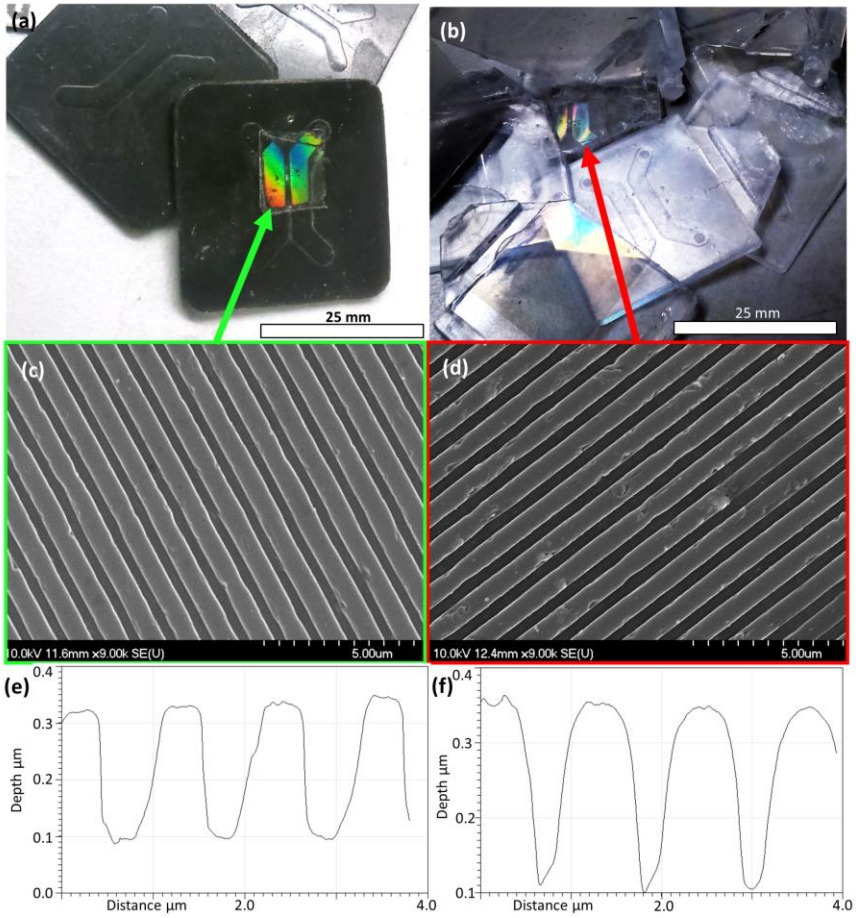

Figure S5. (a) photograph of 3D printed molds in Industrial Blend 1B resin from Fun To Do featuring a 240 nm deep, 500 nm wide grating on 1.25 µm pitch. (b) injection molded polystyrene replicas of the molds in part (a). (c-d) electron micrographs depicting the nanogratings of parts (a) and (b) respectively. (e-f) AFM profiles of (c) and (d) respectively.